Article

SOURCE DATA | TRANSPARENT PROCESS

THE EMBO JOURNAL

Presynaptic inhibition upon CB1 or mGlu2/3 receptor activation requires ERK/MAPK phosphorylation of Munc18-1

Sabine K Schmitz[1,†], Cillian King[1,†], Christian Kortleven[2], Vincent Huson[1], Tim Kroon[2], Josta T Kevenaar[1], Desiree Schut[1], Ingrid Saarloos[1], Joost P Hoetjes[1], Heidi de Wit[1], Oliver Stiedl[1,3], Sabine Spijker[3], Ka Wan Li[3], Huibert D Mansvelder[2], August B Smit[3], Lennart Niels Cornelisse[1], Matthijs Verhage[1,*] & Ruud F Toonen[1,**]

Abstract

Presynaptic cannabinoid (CB1R) and metabotropic glutamate receptors (mGluR2/3) regulate synaptic strength by inhibiting secretion. Here, we reveal a presynaptic inhibitory pathway activated by extracellular signal-regulated kinase (ERK) that mediates CB1R- and mGluR2/3-induced secretion inhibition. This pathway is triggered by a variety of events, from foot shock-induced stress to intense neuronal activity, and induces phosphorylation of the presynaptic protein Munc18-1. Mimicking constitutive phosphorylation of Munc18-1 results in a drastic decrease in synaptic transmission. ERK-mediated phosphorylation of Munc18-1 ultimately leads to degradation by the ubiquitin–proteasome system. Conversely, preventing ERK-dependent Munc18-1 phosphorylation increases synaptic strength. CB1R- and mGluR2/3-induced synaptic inhibition and depolarization-induced suppression of excitation (DSE) are reduced upon ERK/MEK pathway inhibition and further reduced when ERK-dependent Munc18-1 phosphorylation is blocked. Thus, ERK-dependent Munc18-1 phosphorylation provides a major negative feedback loop to control synaptic strength upon activation of presynaptic receptors and during intense neuronal activity.

Keywords homeostatic regulation; presynaptic strength; synapse
Subject Categories Neuroscience
DOI 10.15252/embj.201592244 | Received 8 June 2015 | Revised 28 February 2016 | Accepted 2 March 2016 | Published online 7 April 2016
The EMBO Journal (2016) 35: 1236–1250

Introduction

Homeostatic synaptic plasticity allows the brain to respond to changes in neuronal network activity by adaptation of synaptic strength (Pozo & Goda, 2010; Turrigiano, 2011). A major pathway regulating synaptic plasticity in both invertebrates and vertebrates is the extracellular signal-regulated kinase (ERK) pathway (Martin *et al*, 1997; Di Cristo *et al*, 2001; Satoh *et al*, 2007). Typically, stimulation of receptor tyrosine kinases leads to activation of the GTP-binding protein Ras that sequentially activates protein kinases Raf, MEK, and ERK1/2, ultimately leading to phosphorylation of ERK1/2 targets (Boulton *et al*, 1991; Gomez & Cohen, 1991; Howe *et al*, 1992; Kyriakis *et al*, 1992). In neurons, ERK activation is required for the induction of long-term potentiation (LTP, English & Sweatt, 1996) and several, mainly postsynaptic, cellular mechanisms have been described that may underlie this (Zhu *et al*, 2002; Harvey *et al*, 2008). In addition to these long-term effects, ERK also controls synaptic output more directly (Kushner *et al*, 2005; Vara *et al*, 2009). The best-studied presynaptic ERK target is synapsin, whose phosphorylation enhances neurotransmitter release and is implicated in learning and memory formation (Jovanovic *et al*, 2000; Kushner *et al*, 2005; Vara *et al*, 2009). To prevent negative consequences of excessive excitation, compensating homeostatic mechanisms exist (Turrigiano *et al*, 1998; Burrone *et al*, 2002; Moulder *et al*, 2006). Multiple lines of evidence point to the involvement of the ERK pathway in such homeostatic mechanisms. For instance, stimulation of presynaptic receptors like the cannabinoid 1 receptor (CB1R) and the metabotropic glutamate receptor 2/3 (mGluR2/3) in synaptic plasticity paradigms leads to activation of ERK (Derkinderen *et al*, 2003; Marsicano *et al*, 2003; Lee *et al*, 2009). At

1 Department of Functional Genomics and Clinical Genetics, Center for Neurogenomics and Cognitive Research, Neuroscience Campus Amsterdam, Vrije Universiteit (VU) and VU Medical Center, Amsterdam, The Netherlands
2 Department of Integrative Neurophysiology, Center for Neurogenomics and Cognitive Research, Neuroscience Campus Amsterdam, Vrije Universiteit (VU) and VU Medical Center, Amsterdam, The Netherlands
3 Department of Molecular & Cellular Neurobiology, Center for Neurogenomics and Cognitive Research, Neuroscience Campus Amsterdam, Vrije Universiteit (VU) and VU Medical Center, Amsterdam, The Netherlands
*Corresponding author. Tel: +31 20 59 86936; Fax: +31 20 598 6926; E-mail: matthijs.verhage@cncr.vu.nl
**Corresponding author. Tel: +31 20 59 86946; E-mail: ruud.toonen@cncr.vu.nl
†These authors contributed equally to this work

the same time, activation of these receptors decreases neurotransmitter release (Kamiya *et al*, 1996; Macek *et al*, 1996; O'Leary *et al*, 1997; Scanziani *et al*, 1997; Barbara *et al*, 2003; Mateo & Porter, 2007; Pinheiro & Mulle, 2008; Kellogg *et al*, 2009). This suggests that inhibitory ERK signaling and corresponding targets exist in the nerve terminal, in addition to the well-described transmitter release enhancing ERK effects via its target synapsin. The identity of these presynaptic target(s) for ERK-dependent inhibition is unknown.

Here, we identify a novel inhibitory ERK pathway with the essential presynaptic protein Munc18-1 as downstream effector. Munc18-1 is required for synaptic vesicles exocytosis (Verhage *et al*, 2000; Südhof & Rothman, 2009; Carr & Rizo, 2010). Munc18-1 synaptic levels correlate with synaptic strength as increased Munc18-1 levels lead to a larger readily releasable pool (RRP) size, whereas reduced levels of Munc18-1 in heterozygous null mutant neurons decrease RRP size and synaptic strength (Toonen *et al*, 2006; Toonen & Verhage, 2007). In addition, PKC-dependent phosphorylation of Munc18-1 is essential for diacylglycerol (DAG)-induced potentiation of synaptic transmission (Wierda *et al*, 2007; Genc *et al*, 2014) and synaptic recruitment of Munc18-1 (Cijsouw *et al*, 2014). Therefore, activity-dependent regulation of Munc18-1 phosphorylation provides a powerful mechanism to control presynaptic output. We show that ERK phosphorylates Munc18-1 *in vivo* after foot shock-induced stress, high neuronal activity, or upon stimulation of several types of presynaptic receptors. Preventing ERK-dependent phosphorylation of Munc18-1 increases RRP size and synaptic strength, whereas phosphorylation results in strongly reduced synaptic strength. Increased neuronal network activity results in ERK-mediated phosphorylation of Munc18-1, which ultimately leads to degradation by the ubiquitin–proteasome system. We show that ERK phosphorylation of Munc18-1 is crucial in inhibitory retrograde signaling pathways in glutamatergic hippocampal neurons that control presynaptic output, such as CB1R- and mGluR2/3-dependent depression of neurotransmitter release.

Results

Munc18-1 is a presynaptic ERK substrate

To identify novel synaptic targets of the ERK pathway, we conducted a mass spectrometry screen from adult rat brain and identified Munc18-1 as potential interactor of extracellular signal-regulated kinases 1 and 2 (hereafter referred to as ERK). Direct interaction between Munc18-1 and ERK1 and ERK2 was confirmed independently, using a yeast two-hybrid assay (Fig 1A). In addition, endogenous Munc18-1 immunoprecipitated with ERK1/2 from embryonic and adult brain lysate (Fig EV1A) and ERK1 and Munc18-1 immunoprecipitated from HEK293T cells co-expressing these proteins (Fig EV1B).

Using *in vitro* kinase assays using alanine mutations of potential ERK phosphorylation sites (PxS/TP) in Munc18-1, we identified S241 as the major ERK phosphorylation site in Munc18-1. A Munc18-1 mutant with S241 and T574 changed to alanine ($M18_{S241A,T574A}$) showed a drastic reduction in radioactive phosphate incorporation compared to wild-type Munc18-1 ($M18_{WT}$, Fig 1B–D). Mutation of S241 ($M18_{S241A}$) was equally effective as ($M18_{S241A,T574A}$), whereas the single T574A mutant did not show a reduction in ERK-dependent phosphorylation (Fig EV1C and D). Hence, ERK binds Munc18-1 *in vivo* and *in vitro* and phosphorylates Munc18-1 at amino acid S241 and, to a much lesser extent, T574. The phosphorylation consensus sequence and the amino acid residues around S241 are highly conserved across species (Fig 1E) and S241 and T574 are in close proximity in the crystal structure of Munc18-1 (Misura *et al*, 2000), localizing to the center of the horseshoe-shaped pocket that binds closed syntaxin (Fig 1F).

ERK phosphorylates Munc18-1 *in vivo*

Several studies have shown that ERK activation plays an important role during plasticity and learning (reviewed in Thomas & Huganir, 2004). Contextual fear learning is known to activate ERK leading to phosphorylation of the synaptic vesicle protein synapsin (Kushner *et al*, 2005). To test whether and when Munc18-1 is phosphorylated by ERK *in vivo*, we subjected mice to a fear-learning paradigm (Fig 2A and B) and analyzed endogenous Munc18-1 phosphorylation in synaptosomes obtained from dorsal and ventral hippocampus. For this, we first generated a phospho-antibody that specifically detected Munc18-1 phosphorylated at the S241 site. Kinase assays using exogenous ERK1 or ERK2 produced a robust phospho-band in $Munc18_{WT.}$ That was greatly diminished in the $M18_{S241A}$ or $M18_{S241A,T574A}$ variants (Fig EV1E–H). Immunoreactivity was also ablated upon addition of the ERK pathway inhibitor PD98059, further confirming Munc18-1 as an ERK1/2 substrate and validating the specificity of this phospho-antibody (see Fig 3C and D).

To discriminate learning-specific changes from those attributable to novelty or stress induced by a foot shock, two additional experimental groups were included (no shock and immediate shock exposure, Fig 2B). Whereas phosphorylation at S241 was almost absent in mice that were placed in the novel environment without foot shock exposure, S241 phosphorylation drastically increased in both dorsal and ventral hippocampus when mice received a foot shock (Fig 2C–F). Induction of synapsin phosphorylation was predominantly found in ventral hippocampus (Fig 2D, G and H), whereas Munc18-1 phosphorylation increased in both ventral and dorsal hippocampus (Fig 2D–F). Immediate and delayed shocks were equally effective in triggering ERK auto-phosphorylation (activating ERK, Fig 2G inset) and eliciting ERK phosphorylation of Munc18-1 and synapsin (Fig 2). This suggests that the main determinant of ERK activation and Munc18-1 and synapsin phosphorylation is shock exposure rather than the associative learning component. Together, these experiments show that the ERK pathway is rapidly and robustly activated *in vivo* in response to intense hippocampal information processing leading to phosphorylation of Munc18-1 at S241.

ERK phosphorylation of Munc18-1 is neuronal network activity dependent

Next, we tested whether alterations in network activity would affect Munc18-1 phosphorylation. We manipulated network activity in acute brain slices and subsequently measured phosphorylation levels in synaptic fractions on Western blots. Increasing network activity by blocking inhibitory transmission with $GABA_A$ receptor blocker Gabazine (10 μM) for 4 h resulted in increased

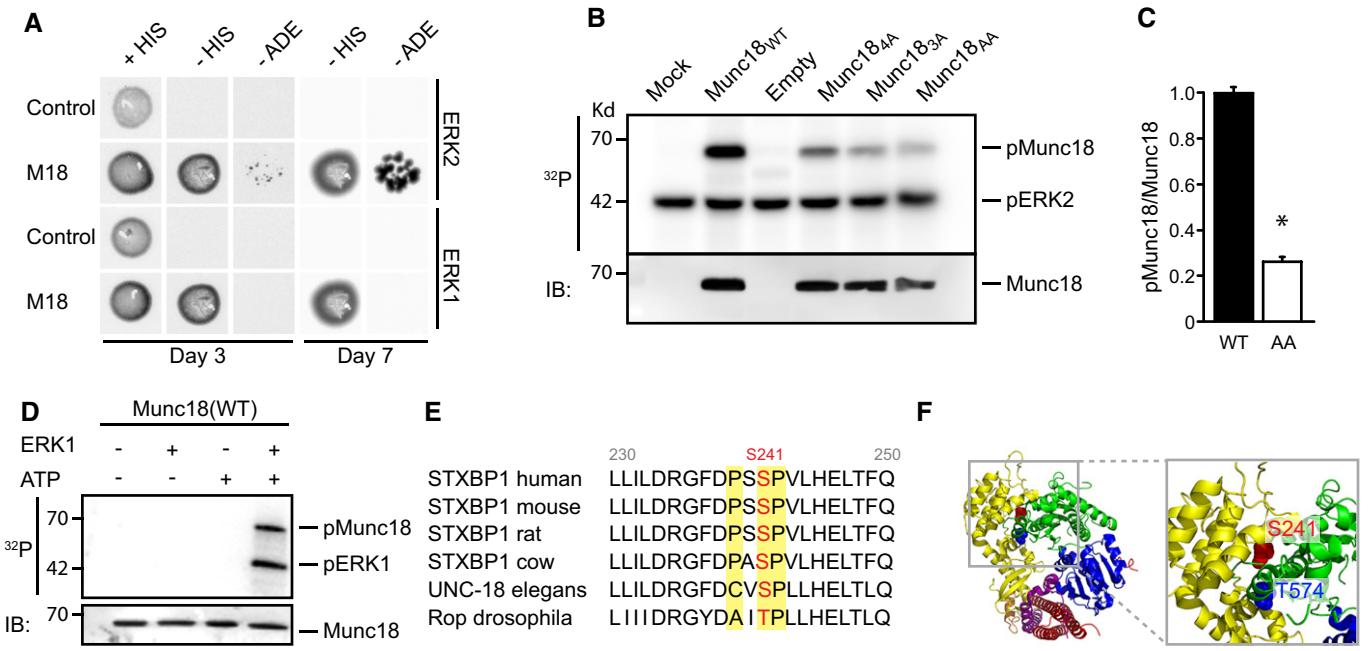

Figure 1. Munc18-1 is an extracellular signal-regulated kinase (ERK) substrate.

A Yeast two-hybrid assays to test for interaction between Munc18-1 and ERK1/2. pGAL4-Munc18-1 (M18) and pGAL4-empty (control) were used as baits and ERK1 and ERK2 as prey. Both ERK1 and ERK2 bind Munc18-1 and allow growth on selection plates [minus histidine (-HIS) and minus adenosine (-ADE)].

B *In vitro* kinase assays showing Munc18-1 phosphorylation by ERK. Radioactive phosphoblot (^{32}P) and immunoblot (IB) of *in vitro* ERK kinase assay using immunoprecipitated Munc18$_{WT}$, Munc18$_{4A}$ (M18$_{T78A,S158A,S241A,T574A}$), Munc18$_{3A}$ (M18$_{S158A,S241A,T574A}$), and Munc18$_{AA}$ (M18$_{S241A,T574A}$) from HEK293T cells incubated with recombinant ERK2. The phosphoblot shows phosphorylated Munc18-1 (pMunc18-1) and auto-phosphorylated ERK2 (pERK2).

C Quantification of phospho-Munc18-1 intensity in wild-type and Munc18$_{AA}$ mutant expressed as the amount of ^{32}P incorporation in Munc18-1 normalized to total Munc18-1 levels. Phosphorylation of Munc18$_{WT}$ was set to 100% (Munc18$_{WT}$: 100 ± 3%; Munc18$_{AA}$: 24 ± 2%, n = 3, *P = 0.01). Mean values ± SEM, unpaired t-test.

D ERK1 *in vitro* kinase assay showing ERK-dependent ^{32}P incorporation in Munc18$_{WT}$ immunoprecipitated from HEK293T cells. Western blot stained with Munc18-1 antibody shows total precipitated Munc18-1 levels were identical in all conditions.

E Alignment of amino acid sequence of Munc18-1 in different species. ERK consensus site (P-X-S/T-P) (yellow) around phosphorylation site S241 (red) is highly conserved.

F Three-dimensional structure of Munc18-1 (blue, green, and yellow ribbons) and syntaxin 1 (purple and red ribbons). Zoom (right) of gray box in full structure (left) illustrates position of the ERK phosphorylation sites S241 (red) and T574 (blue). The T574 site has been reported as phosphorylation site for Cdk5 (Shuang *et al*, 1998).

phosphorylation of Munc18-1 at S241. In contrast, silencing the network with the sodium channel blocker TTX (2 μM) for 4 h resulted in a lower level of phosphorylated Munc18-1 (Fig 3A and B). All treatments were sensitive to inhibition of the ERK pathway, as application of the MEK inhibitor PD98059 resulted in a complete absence of Munc18-1 phosphorylation (Fig 3C and D). Addition of the proteasome blocker MG132 (10 μM) increased levels of phosphorylated Munc18-1 indicating that phosphorylated Munc18-1 becomes a substrate for degradation by the proteasome (Fig 3C and D).

To test whether Munc18-1 is a substrate in pathways that have been implicated in retrograde signaling or homeostatic plasticity, we activated presynaptic receptors upstream of the ERK pathway in the presence of 2 μM TTX (Ferraguti *et al*, 1999; Hartmann *et al*, 2001; Kellogg *et al*, 2009). Application of the TrkB receptor agonist BDNF (100 ng/ml, 48 h) or the mGluR2/3 agonist LY379268 (1 μM, 5 min) increased phosphorylation of Munc18-1 (Fig 3E). Thus, ERK-dependent phosphorylation of Munc18-1 is triggered by increased network activity and by activation of presynaptic receptors that are implicated in negative feedback signaling.

ERK-dependent phosphorylation of Munc18-1 controls synaptic transmission

To investigate whether ERK-dependent Munc18-1 phosphorylation affects synaptic transmission, we rescued *Munc18-1* null mutant autaptic neurons with non-phosphorylatable Munc18-1 (M18$_{S241A}$), phospho-mimicking Munc18-1 (M18$_{S241D}$), or wild-type Munc18 (M18$_{WT}$) as control. First, we analyzed neurons in which ERK cannot phosphorylate Munc18-1 (M18$_{S241A}$). M18$_{S241A}$ had similar synapse number, size and localization, dendrite length, and branching as null mutant neurons expressing wild-type Munc18-1 (M18$_{WT}$, Fig EV2A–G).

Ultra-structural analysis using electron microscopy confirmed this observation and in addition showed that structural features (length of active zone and postsynaptic density), vesicle numbers, and the number of docked vesicles were unchanged in M18$_{S241A}$-expressing neurons (Fig EV3). Together, these data show that M18$_{S241A}$ neurons were morphologically similar to M18$_{WT}$ neurons.

Analysis of synaptic transmission using patch clamp electrophysiology revealed that M18$_{S241A}$-rescued neurons have an almost

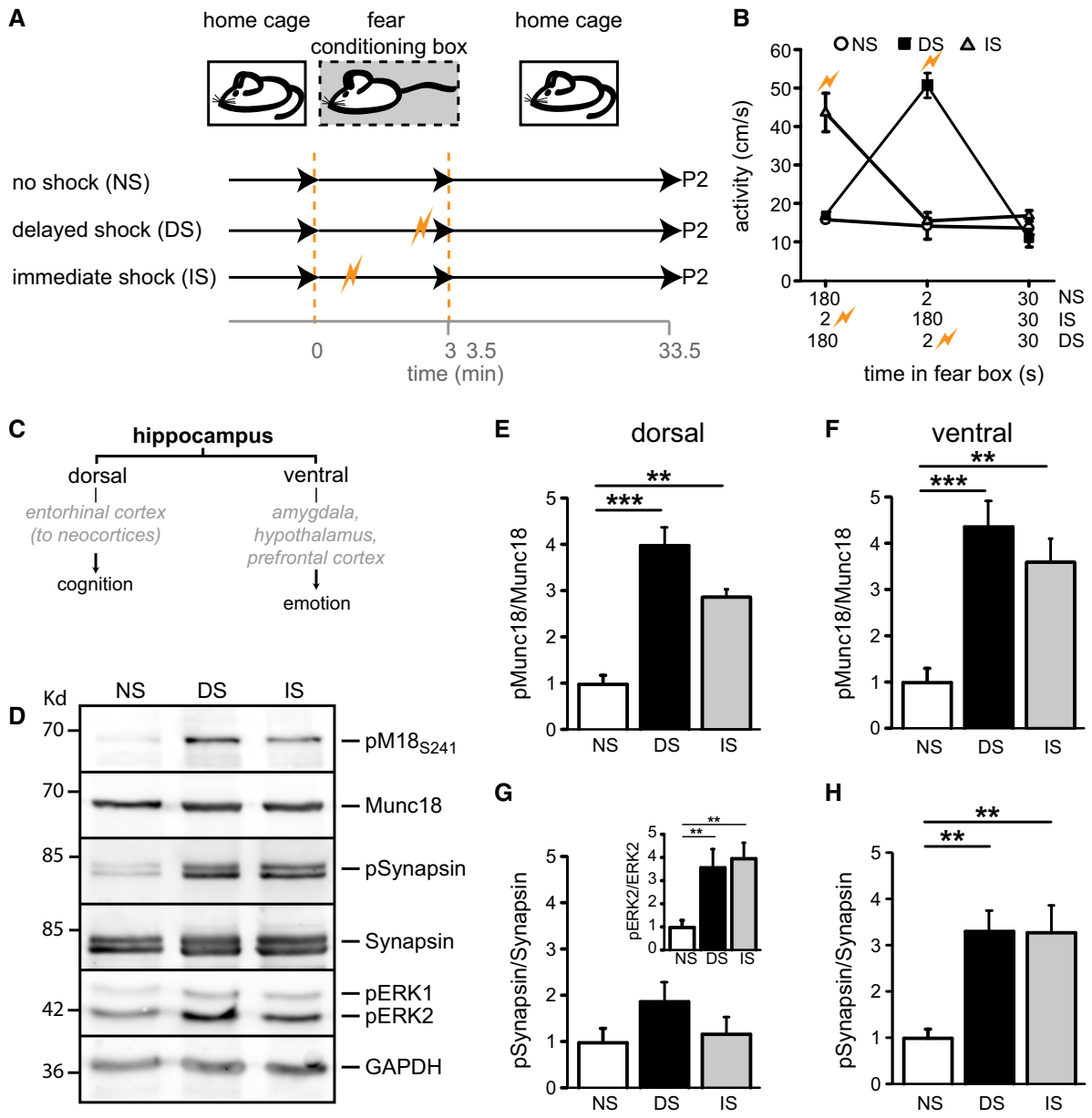

Figure 2. ERK phosphorylates Munc18-1 at S241 *in vivo*.

A Experimental setup of fear-conditioning paradigm. Mice placed in a fear-conditioning box received no shock (NS), an immediate shock (IS), or delayed shock (DS) and were decapitated 30 min after returning to the home cage. Dorsal and ventral hippocampi were subjected to cellular fractionation (P2). DS and IS significantly increased the levels of phosphorylated ERK1/2, a hallmark of ERK activation.

B Activity values across three different training paradigms to ascertain that foot shock was received in the IS and DS group.

C Simplified schematic representation of dorsal and ventral hippocampal connections and their main functions (see Fanselow & Dong, 2010).

D Western blot analysis of P2 synaptosomal fractions of ventral hippocampi from the fear-conditioning paradigm stained for $pM18_{S241}$, total Munc18-1, pSynapsin, total synapsin, pERK, and GAPDH as loading control.

E Quantification of Munc18-1 phosphorylation in dorsal hippocampus expressed as ratio $pM18_{S241}$ over total Munc18-1 levels. No shock was set to 1 (NS: 1.0 ± 0.19, n = 5; DS: 4.01 ± 0.39, n = 5; IS: 2.88 ± 0.37, n = 5; $^{**}P < 0.01$; $^{***}P < 0.001$, one-way ANOVA).

F Quantification of Munc18-1 phosphorylation in ventral hippocampus expressed as ratio $pM18_{S241}$ divided by total Munc18-1 levels (NS: 1.0 ± 0.32, n = 5; DS: 4.39 ± 0.55, n = 5; IS: 3.62 ± 0.50, n = 5; $^{**}P < 0.01$; $^{***}P < 0.001$, one-way ANOVA).

G Quantification of synapsin phosphorylation in dorsal hippocampus expressed as ratio pSynapsin divided by total synapsin levels (NS: 1.0 ± 0.31, n = 5; DS: 1.88 ± 0.43, n = 5; IS: 1.18 ± 0.34, n = 5; n.s.). Inset shows quantification of ERK2 phosphorylation in dorsal hippocampus expressed as ratio pERK2 divided by total ERK2 levels (NS: 1.0 ± 0.11, n = 5; DS: 3.51 ± 0.41, n = 5; IS: 3.98 ± 0.24, n = 5; $^{**}P < 0.01$, one-way ANOVA).

H Quantification of synapsin phosphorylation in ventral hippocampus expressed as ratio pSynapsin divided by total synapsin levels (NS: 1.0 ± 0.20, n = 5; DS: 3.32 ± 0.46, n = 5; IS: 3.30 ± 0.60, n = 5; $^{**}P < 0.01$, one-way ANOVA).

Data information: All data are expressed as mean ± SEM.
Source data are available online for this figure.

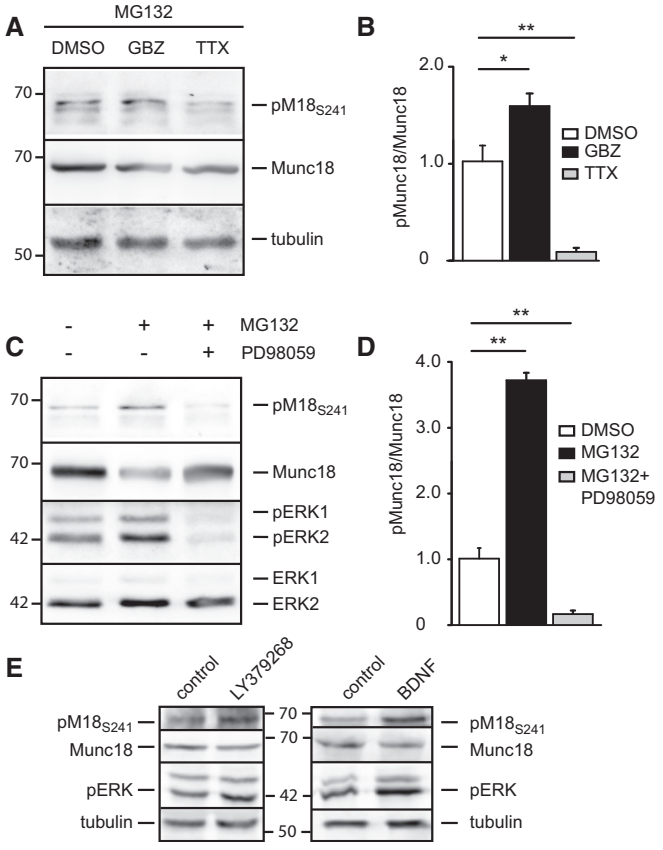

Figure 3. ERK phosphorylates Munc18-1 during increased network activity.

A Western blot of whole-cell lysate of adult mouse brain slices treated with the proteasome inhibitor MG132 (10 μM) and DMSO, the $GABA_A$ receptor blocker Gabazine (GBZ, 10 μM), or the voltage-gated sodium channel blocker TTX (2 μM) for 4 h. Blots were stained for $pMunc18_{S241}$, Munc18-1, and tubulin as loading control.

B Quantification of (A). ERK phosphorylation of Munc18-1 in adult mouse brain slices expressed as ratio $pM18_{S241}$ divided by total Munc18-1 levels. Vehicle (DMSO) was set to 1 (DMSO: 100 ± 0.4%; GBZ: 1.73 ± 0.12; TTX: 0.052 ± 0.002, $n = 4$, $^*P < 0.05$, $^{**}P < 0.01$, one-way ANOVA).

C Western blot of whole-cell lysate of adult mouse brain slices treated with proteasome inhibitor MG132 (10 μM) and MEK inhibitor PD98059 (10 μM) for 4 h. Proteasome block increases the levels of phosphorylated Munc18-1 and ERK1/2, which can be prevented by MEK inhibition. Blots were stained for $pMunc18_{S241}$, Munc18, pERK1/2, and ERK1/2.

D Quantification of (C). ERK phosphorylation of Munc18-1 in adult mouse brain slices expressed as ratio $pM18_{S241}$ divided by total Munc18-1 levels. Vehicle (DMSO) was set to 1 (DMSO: 100 ± 0.8%; MG132: 375 ± 14.2%; MG132 + PD98059: 24 ± 3%, $n = 3$, $^{**}P < 0.01$, one-way ANOVA).

E DIV14 rat cortical cultures treated with type 2 mGluR2/3 agonist LY379268 (1 μM) for 5 min or BDNF (100 ng/ml) for 48 h in the presence of 2 μM TTX and stained for $pMunc18_{S241}$, Munc18, pERK, and tubulin as loading control.

Data information: Data points are mean ± SEM.
Source data are available online for this figure.

twofold increase in evoked postsynaptic current (EPSC) amplitude compared to neurons rescued with $M18_{WT}$ (Fig 4A). Synaptic transmission was also more reliable as the percentage of failures to produce an EPSC upon stimulation was reduced to 0% in neurons expressing $M18_{S241A}$ compared to approximately 15% in $M18_{WT}$-rescued neurons (Fig 4B). Spontaneous release (miniature EPSC) frequency was significantly higher in $M18_{S241A}$ mutants with no effect on mEPSC amplitude (Fig 4C and D). Thus, preventing ERK-dependent phosphorylation of Munc18-1 resulted in a gain-of-function phenotype with increased synaptic transmission.

In contrast, EPSC amplitudes in neurons expressing the phospho-mimicking variant-1 ($M18_{S241D}$) were approximately 6-fold lower than in $M18_{WT}$-rescued neurons (Fig 4A) and spontaneous release frequency showed a more than 10-fold reduction with slightly smaller amplitudes compared to $M18_{WT}$ (Fig 4C–E). Also, about 60% of the neurons failed to respond to electrical stimulation (Fig 4B). $M18_{S241D}$-rescued neurons were smaller than $M18_{WT}$ neurons and had a 25% reduction in the number of synapses (Fig EV2A–D). Synapse size was increased in $M18_{S241D}$ neurons (Fig EV2E) and ultra-structural analysis showed that synapses contained more synaptic vesicles (Fig EV3C) had increased length of the active zone (Fig EV3E) and postsynaptic density (Fig EV3F) as well as a larger cluster size (Fig EV3G).

We probed the size of the readily releasable vesicle pool (RRP) by application of 500 mM hyperosmotic sucrose solution (Rosenmund & Stevens, 1996). RRP size in $M18_{S241A}$ neurons was significantly larger than in $M18_{WT}$ neurons (Fig 4F), while RRP size was too small to be determined reliably in $M18_{S241D}$ neurons. Stimulation with paired pulses of varying inter-stimulus intervals resulted in robust paired-pulse facilitation in $M18_{S241D}$ neurons, indicative of a lower initial release probability in $M18_{S241D}$ neurons (Fig 4G). Paired-pulse ratios in $M18_{S241A}$ neurons were similar to $M18_{WT}$-rescued neurons showing that the release of a single vesicle did not deplete the RRP enough to cause paired-pulse depression (Sullivan, 2007).

Hence, phosphorylation of Munc18-1 at S241 controls basal synaptic transmission: Preventing phosphorylation increases RRP size and synaptic strength, whereas mimicking long-term phosphorylation reduces synaptic strength.

$Munc18_{S241D}$-rescued neurons have lower Munc18-1 levels

We have previously shown that Munc18-1 functions in a dose-dependent manner to control synaptic strength (Toonen *et al*, 2006). To investigate whether the observed electrophysiological properties could be explained by differences in Munc18-1 protein levels or localization, we analyzed synaptic Munc18-1 levels in immunofluorescence images of *Munc18-1* null mutant neurons rescued with the different Munc18-1 constructs (Schmitz *et al*, 2011). As viral expression of Munc18-1 in glia cells prevented accurate assessment of neuronal Munc18-1 levels, we measured Munc18-1 protein levels in neurons grown in the absence of glia. $M18_{S241A}$ neurons had similar Munc18-1 levels as $M18_{WT}$ neurons, while Munc18-1 levels in $M18_{S241D}$ neurons were significantly decreased (Fig 5A–D). As spontaneous activity in these cultures is low and ERK is not frequently activated (Vara *et al*, 2009), we next tested whether increased network activity would affect Munc18-1 protein levels by increasing cell density three-fold or by adding the $GABA_A$ receptor antagonist bicuculline (40 μM, 48 h) to hippocampal mass cultures, which activates the ERK pathway (see Fig 3A and B). Both treatments resulted in a reduction of $M18_{WT}$ levels at synapses compared to synaptic $M18_{S241A}$ levels (Fig 5E

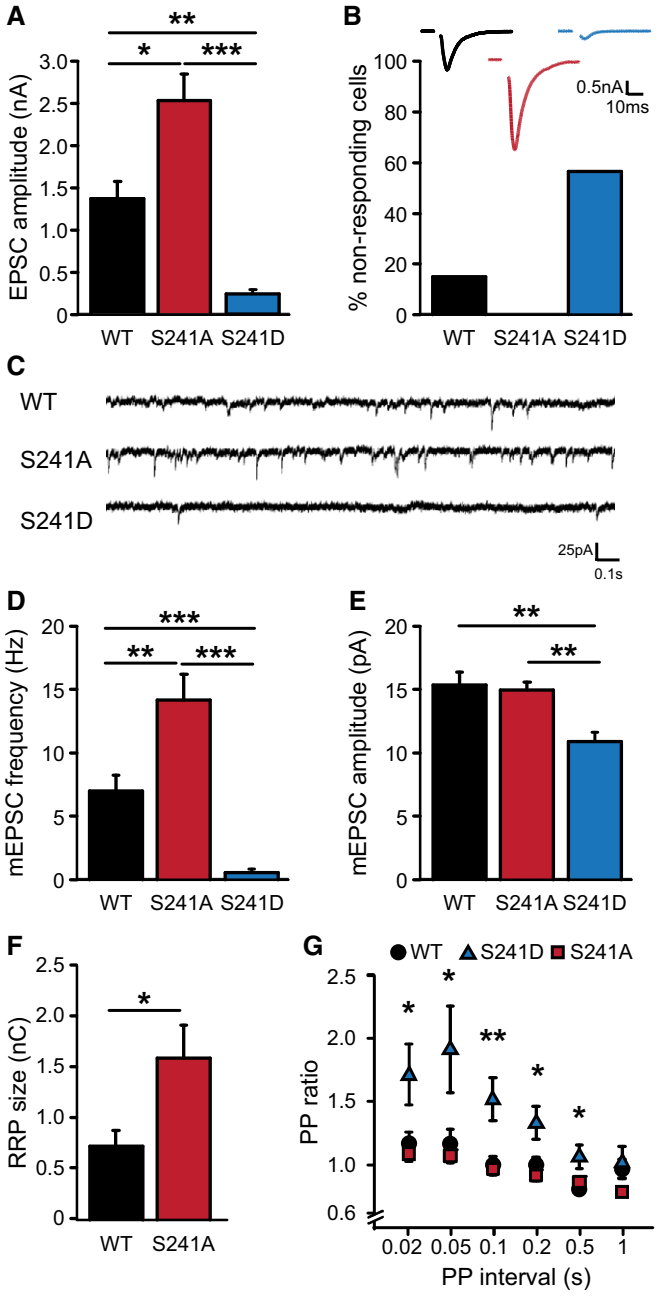

Figure 4. ERK-dependent phosphorylation of Munc18-1 controls synaptic transmission.

Hippocampal autaptic neurons of Munc18-1 null mutant mice were rescued with lentiviruses expressing $M18_{WT}$, $M18_{S241A}$, or $M18_{S241D}$. Electrophysiological recordings were performed between DIV14 and DIV17.

A Amplitude of excitatory synaptic response (EPSC) ($M18_{WT}$: 1.37 ± 0.21 nA, n = 35; $M18_{S241A}$: 2.53 ± 0.31 nA, n = 45; $M18_{S241D}$: 0.24 ± 0.05 nA, n = 17, ***P < 0.001, **P < 0.01, *P < 0.05, Kruskal-Wallis test).

B Percentage of cells that do not respond to electrical stimulation ($M18_{WT}$: 15.5%; $M18_{S241A}$: 0%; $M18_{S241D}$: 56.9%). These cells are not included in (A). Insert: representative recording of single EPSCs. Scale bar represents 10 ms and 0.5 nA.

C Typical examples of spontaneous vesicle release. Scale bar represents 0.1 s and 25 pA.

D Spontaneous release frequency ($M18_{WT}$: 7.05 ± 1.28 Hz, n = 32; $M18_{S241A}$: 14.26 ± 2.04 Hz, n = 37; $M18_{S241D}$: 0.64 ± 0.29 Hz, n = 11; ***P < 0.001, **P < 0.01, Kruskal-Wallis test).

E Amplitude of spontaneous release events ($M18_{WT}$: 15.40 ± 1.06 pA, n = 17; $M18_{S241A}$: 15.03 ± 0.61 pA, n = 20; $M18_{S241D}$: 10.98 ± 0.72 pA, n = 10; **P < 0.01, Kruskal-Wallis test).

F Size of the readily releasable pool (RRP) assessed with single hyperosmotic sucrose application (500 mM, 3.5 s, $M18_{WT}$: 0.74 ± 0.15 nC, n = 7; $M18_{S241A}$: 1.6 ± 0.33 nC, n = 10; $M18_{S241D}$: could not be determined; *P < 0.05, Mann–Whitney U-test).

G Neurons were stimulated with two consecutive pulses with varying inter-stimulus interval to assess release probability. Paired-pulse ratio calculated as ratio of the second to the first synaptic response is plotted as function of inter-stimulus interval ($M18_{WT}$, n = 25; $M18_{S241A}$, n = 19; $M18_{S241D}$, n = 17; *P < 0.05, **P < 0.01, Kruskal-Wallis test).

Data information: All data are expressed as mean ± SEM. See also Figs EV2 and EV3.

and F). Hence, long-term activation of the ERK pathway reduces synaptic Munc18-1 levels, which can be prevented by blocking ERK-dependent phosphorylation of Munc18-1.

Cellular syntaxin levels depend on the presence of Munc18-1 and scale with Munc18-1 expression levels (Toonen *et al*, 2005, 2006). In line with this, syntaxin levels were decreased in $M18_{S241D}$-rescued neurons. Syntaxin levels in $M18_{S241A}$ neurons were higher, suggesting that this Munc18 variant supported syntaxin stability better than wild-type Munc18 (Figs 5G and EV2H–K).

$M18_{S241D}$ levels were lower in all synapses irrespective of their distance from the cell soma and no accumulations were found in the cell indicating that $M18_{S241D}$ is not retained in the Golgi network (Fig 5D). Also when expressed in heterologous HEK293T cells, $M18_{S241D}$ localization was indistinguishable from $M18_{WT}$ (Appendix Fig S1). These experiments show that the lower levels of $M18_{S241D}$ in neurons are not caused by general protein misfolding or transport defects, but instead suggest that $M18_{S241D}$ may be subject to active proteolytic breakdown.

ERK-dependent phosphorylation at S241 primes Munc18-1 for proteasomal degradation

We assessed whether ERK1/2-mediated phosphorylation of Munc18-1 at S241 triggers $M18_{S241D}$ turnover through the ubiquitin–proteasome pathway. We applied the proteasome inhibitor MG132 (10 μM for 6 h) to high-density cultures of *Munc18-1*-deficient neurons expressing $M18_{WT}$, $M18_{S241A}$, or $M18_{S241D}$. Similar to Fig 5E, $M18_{S241A}$ levels in these cultures are higher than $M18_{WT}$. Inhibition of proteasome-dependent degradation resulted in an approximately two-fold increase in $M18_{WT}$ protein levels, whereas $M18_{S241D}$ levels increased more than seven-fold (Fig 5H and I), suggesting that the lower Munc18-1 levels in $M18_{S241D}$ neurons are due to $M18_{S241D}$ degradation by the proteasome.

Poly-ubiquitination is essential for timely recognition and degradation of proteins by the proteasome. To show directly that $M18_{S241D}$ is a proteasome substrate, we assessed the level of poly-ubiquitination of the different Munc18-1 mutants in HEK293T cells which co-expressed HA-tagged ubiquitin. Immunoprecipitated $M18_{S241D}$ but not $M18_{WT}$ or $Munc18_{S241A}$ showed strong HA immunoreactivity, indicating that $Munc18_{S241D}$ is indeed ubiquitinated (Fig 5J and K). Hence, ERK-dependent phosphorylation of Munc18-1 at S241 primes Munc18-1 for ubiquitination and subsequent degradation by the proteasome.

Figure 5. $Munc18_{S241D}$ expression levels are reduced due to proteasomal degradation.

A–F Munc18-1 protein levels were measured in glia-free cultures of Munc18-1 null mutant neurons expressing $M18_{WT}$, $M18_{S241A}$, or $M18_{S241D}$. (A) Typical examples showing Munc18-1 protein localization and intensity in neurites of $M18_{WT}$, $M18_{S241A}$, or $M18_{S241D}$ neurons. MAP2 in blue, VAMP2 in red, and Munc18-1 in green. Scale bar represents 2 μm. (B) Mean somatic Munc18-1 intensity ($M18_{WT}$: 1,682 ± 206 a.u., n = 46; $M18_{S241A}$: 1,719 ± 238 a.u., n = 36; $M18_{S241D}$: 582 ± 98 a.u., n = 33; ***$P < 0.001$). (C) Mean synaptic Munc18-1 intensity ($M18_{WT}$: 1,281 ± 161 a.u., n = 46; $M18_{S241A}$: 1,390 ± 180 a.u., n = 36; $M18_{S241D}$: 210 ± 30 a.u., n = 33; ***$P < 0.001$). (D) Mean synaptic Munc18-1 intensity as a function of radial distance from the soma in neurons described in (B, C). (E) Mean synaptic Munc18-1 intensity in cultures with 3 times the standard number of neurons to increase network activity ($M18_{WT}$: 1,072 ± 123 a.u., n = 36; $M18_{S241A}$: 1,480 ± 170 a.u., n = 32; $M18_{S241D}$: 251 ± 70 a.u., n = 34; *$P < 0.05$, ***$P < 0.001$). (F) Mean synaptic Munc18-1 intensity in cultures treated with $GABA_A$ receptor antagonist bicuculline (40 μM, 48 h) ($M18_{WT}$: 761 ± 121 a.u., n = 26; $M18_{S241A}$: 1,482 ± 150 a.u., n = 31, **$P < 0.01$).

G Mean synaptic syntaxin intensity in autaptic cultures ($M18_{WT}$: 875 ± 35, n = 51; $M18_{S241A}$: 1,058 ± 42, n = 46; $M18_{S241D}$: 458 ± 19, n = 40; **$P < 0.01$, ***$P < 0.001$).

H Western blot of lysates from high-density neuronal cultures from Munc18-1 null mutant mice rescued with $M18_{WT}$, $M18_{S241A}$, or $M18_{S241D}$. Prior to lysis, cells were treated for 6 h with MG132 (10 μM) or DMSO as control. Western blots were stained for Munc18-1 and tubulin as loading control.

I Quantification of (H). Munc18-1 levels were normalized to tubulin levels. Effect of proteasome inhibition was quantified as ratio between MG132 and DMSO treatment of each mutant ($M18_{WT}$: 1.62 ± 0.41; $M18_{S241A}$: 1.26 ± 0.16; $M18_{S241D}$: 7.53 ± 1.17, n = 3; **$P < 0.01$).

J Ubiquitination of different Munc18-1 mutants in HEK293T cells. Western blot of denatured Munc18-1 immunoprecipitations from cells expressing Munc18-1 mutants and HA-tagged ubiquitin. Prior to lysis, cells were treated for 8 h with MG132 (10 μM). Ubiquitin covalently attached to Munc18-1 can be observed as a smear above the characteristic 68 kD Munc18-1 band on Western blots stained for HA-tag.

K Quantification of immunoprecipitation in (J). Level of Munc18-1 ubiquitination was quantified as ratio of immunoprecipitated ubiquitin and Munc18-1 levels. $M18_{WT}$ was set to 1 ($M18_{WT}$: 1 ± 0.06; $M18_{S241A}$: 0.84 ± 0.57; $M18_{S241D}$: 2.70 ± 0.07, n = 3; **$P < 0.01$).

Data information: All data are expressed as mean ± SEM. (B–G, I and K) One-way ANOVA; (F) t-test.
Source data are available online for this figure.

Preventing ERK-dependent phosphorylation of Munc18-1 also prevents endocannabinoid- and mGluR2/3-induced depression of glutamate release

Finally, we tested whether Munc18-1 phosphorylation is important for known synaptic inhibition principles, such as the endocannabinoid and mGluR2/3 signaling pathways. Endocannabinoids are synthesized postsynaptically during periods of high neuronal activity and activate the presynaptic CB1 receptor (Wilson & Nicoll, 2001, 2002; Wilson *et al*, 2001) to produce presynaptic inhibition (Kellogg *et al*, 2009). In line with previous observations (Derkinderen *et al*, 2003), application of the CB1 receptor agonist WIN55,212-2 (30 s, 5 μM) led to a rapid and transient increase of ERK activity in wild-type hippocampal autaptic cultures (Fig 6A). Brief superfusion of *Munc18-1* null mutant neurons rescued with $M18_{WT}$ with 5 μM WIN55,212-2 led to a rapid reduction of evoked release, with EPSC amplitudes dropping to approximately 40% of initial amplitudes 4 min after agonist application (Fig 6B). In contrast, EPSC amplitudes in $M18_{S241A}$-expressing neurons remained constant for the first 2 min after WIN55,212-2 application after which they declined to reach 80% of initial values after 4 min (Fig 6B). WIN55,212-2 application did not affect mEPSC amplitude but reduced mEPSC frequency by approximately 50% in $M18_{WT}$ neurons, indicating that the observed effects had a presynaptic origin (Fig 6C and D). Superfusion with a 5-fold lower concentration of WIN55,212-2 (1 μM) also resulted in a rapid reduction of EPSC amplitudes to 40% of initial amplitudes (Fig 6E) with paired-pulse ratios rising from 0.94 ± 0.1 at t = 0 to 1.36 ± 0.2 at t = 240 (20-ms interval), indicative of a reduced release probability (Fig 6F). Application of vehicle only (DMSO) on $M18_{WT}$-rescued neurons showed a small reduction of EPSC amplitude over time reaching ± 80% of initial values, which is typically observed in prolonged patch clamp recordings and resembles the reduction of EPSC amplitudes upon WIN55,212-2 application on $M18_{S241A}$-rescued neurons (Fig 6E). Application of the CB1 receptor inverse agonist AM251 (1 μM) on $M18_{WT}$ neurons together with the superfusion of WIN55,212-2 prevented the EPSC rundown (Fig 6G).

Acute activation of the mGluR2/3 (Ferraguti *et al*, 1999) and more long-term activation of TrkB receptors (Segal & Greenberg, 1996) also induced ERK activation and Munc18 phosphorylation (Fig 3E). To test whether ERK-dependent phosphorylation of Munc18-1 modulates synaptic transmission upon mGluR2/3 activation, we superfused $M18_{WT}$ or $M18_{S241A}$ autapses with the mGluR2/3 agonist LY379268 (1 μM, 4 min). This caused a reduction of both EPSC amplitude and mEPSC frequency in $M18_{WT}$-rescued neurons (Fig 6H–J, WT n = 11) similar to the reduction observed in wild-type autapses (Bushell *et al*, 1999). In contrast, LY379268 application did not affect evoked and spontaneous release in $M18_{S241A}$-rescued neurons (Fig 6H–J, S241A n = 16). Hence, activation of multiple receptor systems leads to ERK-dependent Munc18 phosphorylation, which reduces synaptic output.

ERK pathway inhibition decreases depolarization-induced suppression of excitation (DSE) and WIN55,212-2-induced depression in cultured neurons and brain slices

To test the effect of MEK/ERK pathway inhibition on different forms of synaptic depression, we applied the MEK/ERK pathway inhibitors PD98059 and/or U0126 in acute hippocampal slices and isolated neurons from wild-type mice. First, we triggered depolarization-induced suppression of excitation (DSE) in CA1 hippocampal neurons by depolarization to 0 mV for 10 s. DSE is a form of short-term synaptic plasticity mediated by endogenous cannabinoid signaling first described in cerebellar excitatory synapses (Kreitzer & Regehr, 2001) and also observed in cultured hippocampal neurons (Ohno-Shosaku *et al*, 2002; Straiker & Mackie, 2005) and hippocampal slices (Ohno-Shosaku *et al*, 2002; Xu *et al*, 2010). PD pretreatment did not affect basal synaptic strength prior to DSE induction (Fig 7A). Depolarization to 0 mV for 10 s (DSE protocol) resulted in a robust depression of EPSC amplitudes (Fig 7B, control n = 10 slices), which recovered in approximately 40 s. However, in hippocampal slices pretreated with PD98059, which almost completely blocked ERK activity (see Fig 3C), DSE was severely reduced and recovery to pre-DSE amplitudes occurred four-fold faster

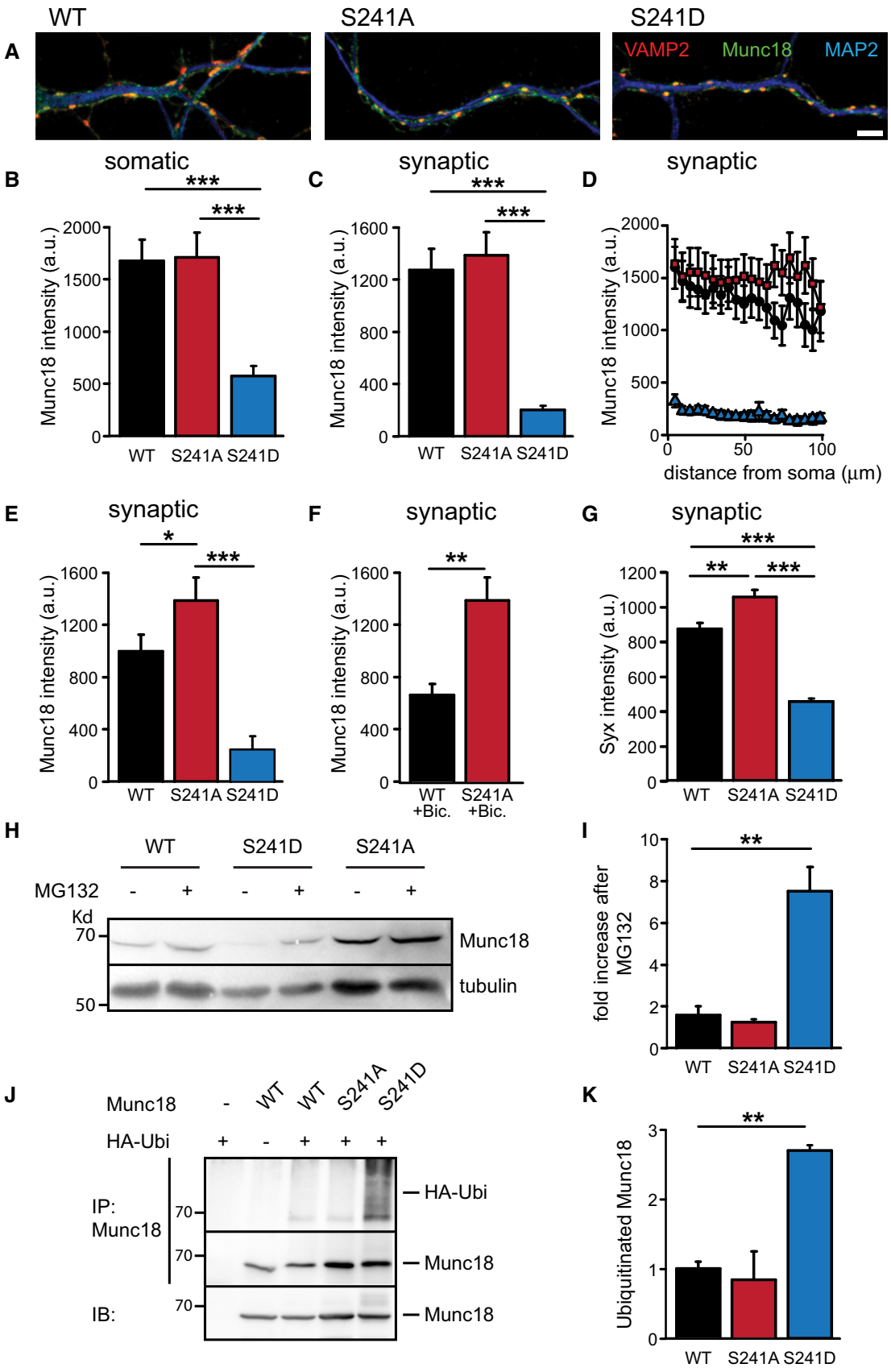

Figure 5.

Figure 6. Munc18-1 functions in endocannabinoid-induced depression of glutamate release.

A Western blot from whole-cell lysate of Munc18-1 null mutant neurons rescued with $M18_{WT}$ and incubated with WIN55,212-2 (5 μM) for 30 s. Cells were harvested after the indicated time. CB1R activation leads to a rapid and transient increase in pERK activity.

B–D Hippocampal autaptic neurons of Munc18-1 null mutant mice were rescued with lentiviruses expressing $M18_{WT}$ or $M18_{S241A}$. CB1R agonist WIN55,212-2 (5 μM) was applied at t = 60 s for 30 s. (B) Amplitude of excitatory synapse response normalized to t = 0 s. Neurons were stimulated by a single action potential every 30 s for 4 min ($M18_{WT}$ n = 21, $M18_{S241A}$ n = 24, *P < 0.05, Mann–Whitney U-test). Note the broken y-axis. (C) Ratio of the frequency of spontaneous release events after (t = 180 s) and before (t = 0 s) WIN55,212-2 application ($M18_{WT}$: 58.0 ± 2.3%, n = 21; $M18_{S241A}$: 84.2 ± 5.6%, n = 24, *P < 0.05, Mann–Whitney U-test). (D) Ratio of amplitude of spontaneous release events after (t = 240 s) and before (t = 0 s) WIN55,212-2 application ($M18_{WT}$: 85.0 ± 2.7%, n = 21; $M18_{S241A}$: 83.1 ± 2.6%, n = 24).

E–G Autaptic neurons of Munc18-1 null mutant mice rescued with lentiviruses expressing $M18_{WT}$ were superfused with WIN55,212-2 (1 μM), WIN55,212-2 (1 μM) plus AM251 (1 μM), or vehicle only (DMSO). (E) Amplitude of excitatory synapse response normalized to t = 0 s. CB1R agonist WIN55,212-2 (1 μM) or vehicle only (DMSO) was applied at t = 60 s for 30 s (WT + WIN n = 13; WT + DMSO n = 16, *P < 0.05, Mann–Whitney U-test). Note the broken Y-axis. (F) Paired-pulse ratio (20 ms interval) at t = 0 and t = 240 s in $M18_{WT}$ neurons superfused with CB1R agonist WIN55,212-2 (1 μM) at t = 60 s for 30 s. WIN55,212-2 application increases PP ratios indicative of a reduction of synaptic release probability (t = 0 s: 0.94 ± 0.1, n = 13; t = 240 s: 1.36 ± 0.2, n = 16, *P < 0.05, Mann–Whitney U-test). (G) Amplitude of excitatory synapse response normalized to t = 0 s. CB1R agonist WIN55,212-2 (1 μM) was applied together with the CB1R antagonist AM251 (1 μM) at t = 60 s for 30 s (WT + WIN n = 13, same trace as 6F; WT + WIN + AM251 n = 15, *P < 0.05, Mann–Whitney U-test). Note the broken Y-axis.

H–J Hippocampal autaptic neurons of Munc18-1 null mutant mice were rescued with $M18_{WT}$ or $M18_{S241A}$. mGluR2/3 agonist LY379268 (1 μM) was applied by bath perfusion for 4 min. (H) Ratio of amplitude of evoked release events after (t = 240 s) and before (t = 0 s) LY379268 application ($M18_{WT}$: 55.0 ± 4.7%, n = 14; $M18_{S241A}$: 81.1 ± 3.6%, n = 16, *P < 0.05, Mann–Whitney U-test). (I) Ratio of frequency of spontaneous release events after (t = 240 s) and before (t = 0 s) LY379268 application ($M18_{WT}$: 63.0 ± 5.7%, n = 14; $M18_{S241A}$: 85.1 ± 3.4%, n = 16, *P < 0.05, Mann–Whitney U-test). (J) Ratio of the amplitude of spontaneous release events after (t = 240 s) and before (t = 0 s) WIN55,212-2 application ($M18_{WT}$: 81.0 ± 1.3%, n = 14; $M18_{S241A}$: 82.1 ± 3.3%, n = 16).

Data information: All data are mean ± SEM.
Source data are available online for this figure.

(within 10 s, Fig 7C, PD-pretreated n = 11). DSE was 31.20 ± 4.8% for wild-type neurons and 12.59 ± 2.1% for PD-pretreated slices (Fig 7D). Hence, blocking the MEK/ERK pathway in hippocampal slices severely reduces DSE.

Secondly, we tested the effect of ERK pathway inhibition on CB1 receptor-induced synaptic depression using the synthetic analog WIN55,212-2. Also here, pretreatment with PD98059 did not affect basal synaptic strength (Fig 7E). Superfusion of 1 μM WIN55,212-2 resulted in a gradual reduction of EPSC amplitudes (Fig 7F, control n = 6 slices) that recovered to baseline within 30 min after WIN washout (Fig EV4A). However, in slices pretreated with ERK pathway inhibitor, WIN55,212-2 superfusion did not induce synaptic depression (Fig 7G, PD-pretreated n = 6 slices). Effect sizes measured 30 min after WIN55,212-2 superfusion showed a 35% reduction of EPSC amplitudes in control slices compared to 6% in PD-pretreated slices (Fig 7H). Hence, blocking the ERK pathway in hippocampal slices abolished CB1R-mediated synaptic depression.

Thirdly, we treated hippocampal autapses with the MEK/ERK pathway inhibitors PD98059 and U0126 for 3 h. Semi-quantitative analysis using phospho-ERK antibodies showed that ERK inhibition did result in reduction of phospho-ERK levels but not in all neurons (Fig EV5A and B). Pretreatment with the MEK/ERK pathway inhibitors (EPI) had no effect on EPSC amplitudes (Fig EV5C). Upon DSE induction in control neurons, a 60% reduction in EPSC amplitudes was observed (Fig EV5D and E, control n = 8 neurons). In contrast, in EPI-pretreated neurons, EPSC amplitudes depressed only by 20% (Fig EV5D and E, EPI n = 7 neurons). Thus, even incomplete ERK inhibition significantly reduces DSE in autaptic neurons, similar to the effect in hippocampal slices.

Finally, we tested the effect of MEK/ERK pathway inhibition on CB1 receptor-induced synaptic depression using the synthetic analog WIN55,212-2 in autapses. WIN55,212-2 (1 μM) application resulted in a strong depression in all neurons (Fig EV5F–H, control = 13 neurons), which reversed within 2 min after WIN55,212-2 washout (Fig EV4B). The extent of depression was similar to the effect observed in $M18_{WT}$ expressing *Munc18-1* null mutant neurons and hippocampal slices. However, ERK pathway inhibition only blocked EPSC depression upon WIN55,212-2 application in a subpopulation of isolated neurons (Fig EV5F–H, EPI n = 15 neurons). In 20% of the neurons pretreated with ERK inhibitors, WIN55,212-2 failed to induce EPSC depression (Fig EV5I), while WIN55,212-2 was effective in all wild-type neurons. The incomplete reduction of phospho-ERK levels upon EPI treatment (Fig EV5A and B) in autapses but not in slices (Fig 3C) may explain the smaller effect of ERK inhibitors in autapses compared to hippocampal slices. Together, the slice and autapse data show that ERK pathway inhibition strongly inhibits DSE amplitude and duration and blocks WIN55,212-2-induced depression in hippocampal slices and in a subset of hippocampal autaptic neurons.

Discussion

The regulation of presynaptic strength is a crucial element in neuronal information processing and memory formation (Abbott & Regehr, 2004). In the present study, we identified a novel presynaptic inhibitory pathway that is activated *in vivo* upon increased hippocampal information processing in a fear-conditioning paradigm and *in vitro* upon high neuronal activity, stimulation of presynaptic receptors involved in homeostatic (inhibitory) feedback mechanisms, and depolarization-induced suppression of excitation (DSE). This pathway controls synaptic strength by ERK-dependent phosphorylation of Munc18-1. We provide evidence that this mechanism functions in CB1R- and mGluR2/3-mediated suppression of glutamate release. We show that acute, short-term adaptations in presynaptic strength are mediated, at least to a substantial extent, by ERK signaling. Together, our findings suggest that ERK-dependent signaling and Munc18-1 phosphorylation provide a major negative feedback loop to control synaptic strength upon activation of presynaptic receptors and during intense neuronal activity.

The ERK pathway is activated by synaptic activity and required for various forms of synaptic plasticity (English & Sweatt, 1996; Martin *et al*, 1997; Di Cristo *et al*, 2001; Zhu *et al*, 2002). In addition to well-established long-term effects, probably targeting the nucleus

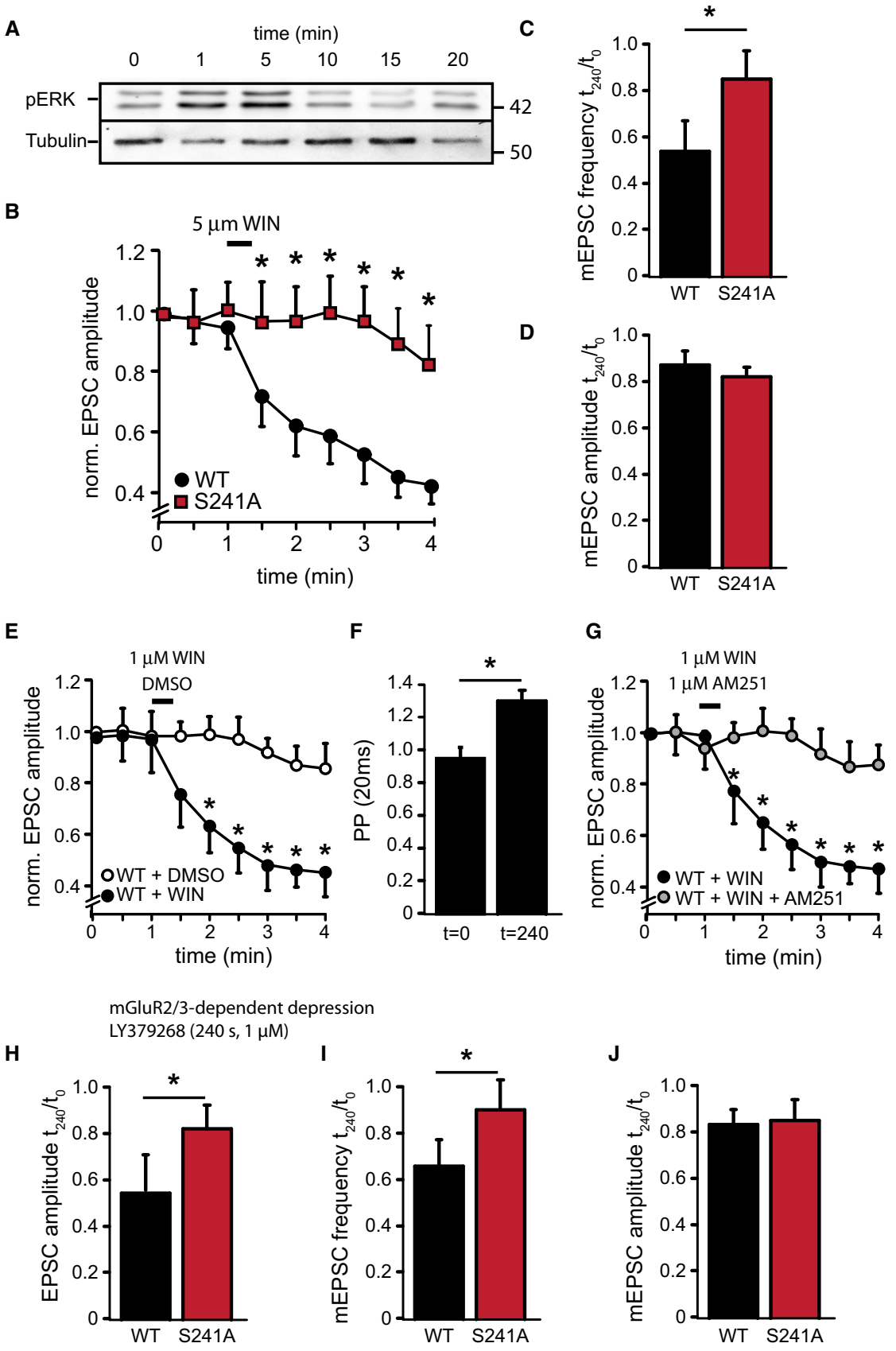

Figure 6.

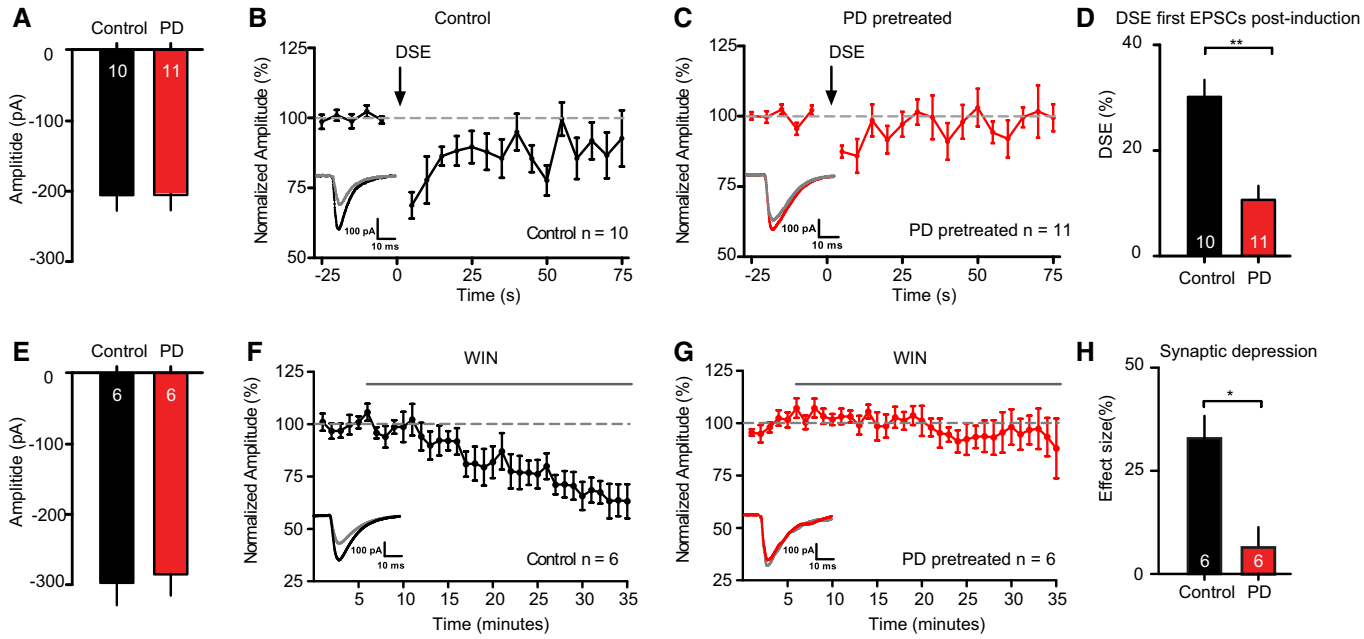

Figure 7. ERK pathway inhibition decreases DSE and WIN55,212-2-induced depression.

A–D DSE duration and amplitude is decreased in CA1 pyramidal neurons upon ERK pathway inhibition by a pretreatment with PD98059 (PD; 10 μM) compared to 0.1% DMSO (control). (A) Average EPSC amplitude during 25-s baseline recording prior to DSE induction shows no significant differences in EPSC amplitude between the DMSO- and PD-pretreated groups (DMSO: 196.36 ± 16.51 pA, n = 10; PD: 196.42 ± 18.61 pA, n = 11, P = 0.9). (B) Average DSE in neurons of DMSO-pretreated slices, induced by a 10-s depolarization to 0 mV (arrow), n = 10. Inset: example traces of 2 averaged EPSCs before (black) and after depolarization (gray). (C) Average DSE in slices pretreated with PD (n = 11). Insets: example traces of 2 averaged EPSCs before (red) and after depolarization (gray). (D) Comparison of DSE between control and PD. PD pretreatment limits amplitude and duration of DSE. **P < 0.01; unpaired t-test with Welch's correction. Numbers in bars represent the number of neurons in each group.

E–H ERK pathway inhibition by pretreatment with PD98059 (PD; 10 μM) blocks the effect of WIN55,212-2 (WIN; 2 μM) on the amplitude of EPSCs recorded in CA1 pyramidal neurons. (E) Average EPSC amplitude during 5-min baseline recording prior to DSE induction shows no significant differences in EPSC amplitude between the DMSO- and PD-pretreated groups (DMSO: 295.69 ± 28.73 pA, n = 6; PD: 270.86 ± 32.14 pA, n = 6, P = 0.6). (F) Effect of WIN application (gray bar, 30 min) on EPSC amplitude in CA1 pyramidal neurons of 0.1% DMSO (control)-pretreated slices (n = 6). Inset: example traces of averaged EPSCs of baseline (black) and the last 5 min (gray). (G) Effect of WIN application (gray bar, 30 min) on EPSC amplitude in CA1 pyramidal neurons of PD-pretreated slices (n = 6). Inset: example traces of averaged EPSCs of baseline (red) and the last 5 min (gray). (H) Comparison of the effect size of the last 5 min in both groups shows a significant difference. *P < 0.05; unpaired t-test. Numbers in bars represent number of slices in each group.

Data information: All data are expressed as mean ± SEM.

and regulating transcription, activated ERK is also present in presynaptic terminals where it acutely phosphorylates synaptic substrates to more directly control synaptic strength (Vara *et al*, 2009). Synapsin I is the best-established ERK substrate in the nerve terminal and its phosphorylation enhances synaptic vesicle mobility (Chi *et al*, 2003) and correlates with long-term potentiation on the timescale of hours to days (Kushner *et al*, 2005). Synapsin phosphorylation is also linked to more acute effects on vesicle release although evidence for the relevance of ERK-dependent synapsin phosphorylation on enhancing glutamate release from isolated synaptosomes is based on PD98059 application (Jovanovic *et al*, 2000), that is, manipulations that block positive as well as negative actions of ERK substrates. To our knowledge, the effect of a phosphorylation-deficient synapsin mutant expressed on a synapsin (triple) null mutant background, like we present here for Munc18-1, has not been performed yet. Hence, the specific contribution of synapsin I phosphorylation to overall synaptic effects of ERK activation remains to be determined. Our data confirm ERK-dependent synapsin phosphorylation, and we show that it occurs during fear conditioning to an almost similar extent as Munc18-1 phosphorylation (Fig 1). Given their abundance, phosphorylation of synapsin and Munc18-1 probably occurs in overlapping populations of synapses. However, the fact that synaptic transmission is enhanced not inhibited upon acute ERK inhibition shows that the net effect of ERK activation is to inhibit synaptic transmission in the synapses studied here (Figs 6, 7 and EV5). Hence, the previously proposed enhancing effect on synapsin phosphorylation is not in place in these synapses on the timescale assessed in the current study or is upstream of the inhibitory effect of Munc18-1 phosphorylation. Munc18-1-dependent inhibition is the dominant effect of ERK activation among the two substrates currently identified and blockade of the entire ERK pathway resulted in a similar phenotype as selective blockade of one ERK substrate (Munc18-1).

Recent studies have identified several inhibitory pathways involving retrograde messengers and metabotropic presynaptic receptors to regulate neurotransmitter release. The endocannabinoid system is one of the most widespread retrograde signaling mechanisms in the brain (Wilson *et al*, 2001; Alger, 2002; Kreitzer & Regehr, 2002; Chevaleyre *et al*, 2006). Activation of CB1 receptors triggers several forms of short- and long-term plasticity including endocannabinoid-induced LTD (eCB-LTD, Chevaleyre *et al*, 2007)

and depolarization-induced suppression of excitation (DSE, Kreitzer & Regehr, 2001; Ohno-Shosaku *et al*, 2002). Multiple downstream effector molecules such as the presynaptic proteins RIM1α and RAB3B, P/Q-type voltage-gated calcium channels (VGCCs), and the cAMP/PKA pathway have been implicated in such presynaptic modulation (reviewed in Heifets & Castillo, 2009; Castillo *et al*, 2012). Endocannabinoid-induced short-term plasticity (eCB-STP) of climbing fiber to Purkinje cell synapses in the cerebellum appears to involve VGCC modulation (Kreitzer & Regehr, 2001). However, CB1 receptors also signal via the ERK pathway (Derkinderen *et al*, 2003; Dalton & Howlett, 2012). We observed that the CB1R pathway in hippocampal neurons and slices also functions to control presynaptic release by activating the ERK pathway and that ERK-dependent Munc18-1 phosphorylation upon acute CB1R activation functions in the initial phase of cannabinoid-induced synaptic depression. ERK-dependent inhibition of release was observed already after 30 s of CB1R activation and was absent in neurons that expressed the non-phosphorylatable form of Munc18-1 and severely reduced after MEK/ERK inhibitors in hippocampal slices and, to a lesser extent, in isolated neurons. Hence, on the timescale of our experiments, ERK-dependent phosphorylation of Munc18-1 is a major mechanism to reduce synaptic release upon activation of CB1 and also mGluR2/3.

This newly identified ERK/Munc18 mechanism most likely works together with other pathways, such as VGCC modulation (Kreitzer & Regehr, 2001). The role of each of these might vary among the different forms of CB1R-dependent presynaptic plasticity. For instance, some synaptic depression remains in the presence of MEK/ERK inhibitors after DSE protocols in slices and isolated neurons (Figs 7C and EV5E), while direct application of CB1R agonist WIN55,212-2 is completely inhibited by MEK/ERK inhibitors in slices (Fig 7F), but only in a subpopulation of isolated neurons (Fig EV5H). In the latter case, this incomplete effect might be due to the fact that ERK itself appears to be activated (more ERK autophosphorylation) and upon addition of inhibitors remains in a phosphorylated state much longer than in hippocampal slices (compare Figs 3C and EV5B).

Munc18-1 is essential for synaptic vesicle release (Verhage *et al*, 2000). The potent modulation of synaptic strength by ERK-dependent Munc18-1 phosphorylation upon CB1R and mGluR2/3 activation confirms that Munc18-1 is also a potent modulator of different forms of synaptic plasticity, as previously shown for diacylglycerol-dependent augmentation (Wierda *et al*, 2007) and post-tetanic potentiation (Genc *et al*, 2014). In the crystal structure of the Munc18-1/syntaxin dimer (Misura *et al*, 2000), S241 is located in the syntaxin 1 binding pocket of Munc18-1. It is therefore conceivable that phosphorylation of S241 negatively affects the Munc18-1/syntaxin interaction and thereby synaptic transmission. Preventing phosphorylation in $M18_{S241A}$ results in increased RRP size and EPSC amplitude arguing that $M18_{S241A}$ is more efficient to drive synaptic transmission than wild-type Munc18-1. In $M18_{S241A}$ autapses, we also observed slightly higher synaptic expression levels of syntaxin 1 suggesting that $M18_{S241A}$ supports syntaxin 1 stability better than wild-type protein. We previously demonstrated that cellular expression levels of Munc18-1 correlate with synaptic strength (Toonen *et al*, 2006) and that neuronal activity dynamically modulates Munc18-1 levels at individual synapses in a PKC-dependent manner (Cijsouw *et al*, 2014). The ubiquitin–proteasome system (UPS) has been implicated in homeostatic plasticity (Ehlers, 2003; Willeumier *et al*, 2006; Jiang *et al*, 2010; Rinetti & Schweizer, 2010; Lazarevic *et al*, 2011). Expression of $M18_{S241D}$ in *Munc18-1* null mutant neurons, mimicking prolonged ERK-dependent Munc18-1 phosphorylation, eventually leads to ubiquitination and proteasomal degradation of Munc18-1 resulting in an almost complete blockade of synaptic transmission. Not surprisingly, synapses in the phosphomimicking mutant displayed typical morphological features as observed upon network silencing by TTX application (Murthy *et al*, 2001). In contrast, we observed higher Munc18-1 levels upon prolonged increased network activity in neurons expressing the non-phosphorylatable form of Munc18-1 ($M18_{S241A}$) compared to wild-type Munc18-1. Hence, in addition to the acute effects of ERK-dependent phosphorylation of Munc18-1 on synaptic transmission, this pathway may also function in more long-term homeostatic mechanisms via controlling synaptic Munc18-1 expression levels.

Together, our data reveal a novel presynaptic inhibitory pathway of ERK-dependent Munc18-1 phosphorylation that acts to temporarily reduce synaptic transmission upon acute activation of presynaptic CB1 and mGlu2/3 receptors. Long-term activation of this pathway ultimately leads to degradation of ERK-phosphorylated Munc18-1 via ubiquitination and proteasomal breakdown.

Materials and Methods

Mouse mutant strains and generation of lentiviral particles

Munc18-1 null mutant mice were generated as described (Verhage *et al*, 2000). E18 embryos were collected by cesarean section from pregnant females from timed heterozygous mating. Newborn P0–P1 Wistar rats (Harlan) were used for glia preparations. Animals were housed and bred according to Dutch governmental guidelines. All animals were handled according to approved VU University Animal Ethics and Welfare Committee protocols (DEC-FGA-13-03 and DEC-FGA-14-01). Generation of lentiviral constructs, generation of virus stocks, and neuron infections were performed as published (Wierda *et al*, 2007). See Appendix Supplementary Methods for details.

Antibodies and chemicals

A detailed description of reagents and antibodies is included in Appendix Supplementary Methods.

Protein interactions studies

Yeast two-hybrid studies were performed using the MATCHMAKER Two-Hybrid System 3 (Clontech). Munc18-1 fused to GAL4 DNA-binding domain was used as bait. As prey, ERK1 or ERK2 cDNA was fused to the GAL4 transcription activation domain. Yeast growth selection on synthetic media (−ADE and −HIS) was performed in accord with the manufacturer's protocol. Mass spectrometry on brain P2 fractions was performed as described (Li *et al*, 2007). See Appendix Supplementary Methods for details.

Cell culture and electrophysiology

For quantification of Munc18-1 levels, embryonic medium-density (100,000 cells/12 well) or high-density (300,000 cells/12 well)

hippocampal cultures from *Munc18-1* null mutant mice were grown on glass coverslips coated with poly-D-lysine (40 μg/ml) and laminin (2.5 μg/ml) (BD Biosciences). For Munc18-1 phosphorylation assays, wild-type hippocampal neurons were plated onto poly-D-lysine and laminin-coated 6-cm dishes at 1.5×10^6 cells per dish.

Autaptic neuronal culture and electrophysiological recordings were performed as described (Toonen *et al*, 2006; Wierda *et al*, 2007; Weber *et al*, 2010). Hypertonic sucrose to assess RRP size (500 mM, 4 s) and WIN55,212-2 (1 and 5 μM, 30 s) was applied via a fast switching dual-barrel application system (Warner Instruments). LY379268 (1 μM) was applied via bath perfusion. Depolarization-induced suppression of excitation (DSE) was induced according to Straiker and Mackie (2005): 20 s after a 0.5 Hz baseline, neurons were depolarized to 0 mV for 10 s, after which test pulses were applied at 0.5 Hz for 100 s. ERK pathway inhibitors were applied in the 37°C incubator 0.5 h prior to recordings and remained present throughout the recording. See Appendix Supplementary Methods for details.

Hippocampal slice preparation and electrophysiology

Mouse hippocampal coronal slices (300–350 μm) were prepared from P22–26 male and female C57BL/6 mice. Slices were placed in the recording chamber and perfused with aCSF (1.5–2 ml/min, osmolality of ± 300 mOsm) at 32 ± 1°C. Hippocampal CA1 pyramidal neurons were patched and EPSCs were evoked by stimulating the CA3 to CA1 Schaffer collateral. For depolarization-induced suppression of excitation (DSE) experiments, slices were perfused with aCSF with 0.1% DMSO or 10 μM of PD98059. 2 μM of SR95531 (Gabazine) was added to block GABA-A-mediated inhibitory responses. EPSCs were evoked at 0.2 Hz for a minimum of 25 s baseline after which the cell was depolarized to 0 mV for 10 s. Immediately after, EPSCs were evoked at 0.2 Hz at −70 mV and responses recorded for 75 s (15 EPSCs). This experiment was repeated after 3 min post-depolarization, when EPSCs had returned to baseline to obtain 2 DSE experiments from each cell. EPSC amplitude was normalized to baseline of each individual experiment and averaged over two experiments to result in one averaged normalized result per cell. To evaluate the effect of the CB1 receptor agonist WIN55,212-2 (WIN), slices were perfused with aCSF with 0.1% DMSO or 10 μM of PD98059. 2 μM of SR95531 (Gabazine) was added to block GABA-A-mediated inhibitory responses, as well as 200 nM of the A1 adenosine receptor antagonist 8-cyclopentyl-1,3-dipropylxanthine (DPCPX). EPSCs were evoked at 0.1 Hz for a minimum of 5 min baseline, before 30 min WIN (2 μM) application. All drugs used were diluted in DMSO. 8-cyclopentyl-1,3-dipropylxanthine (DPCPX; 200 nM) was from Tocris (UK) and SR95531 hydrobromide (Gabazine; 2 μM) from Hello Bio (UK). See Appendix Supplementary Methods for details.

Fear-conditioning training

Male 10-week-old C57BL/6J mice (Charles River) were divided randomly into three groups (no shock control (NS), immediate shock (IS), and delayed shock (DS); $n = 5$ per group). Fear-conditioning training was done as published (Wiltgen *et al*, 2001; Stiedl *et al*, 2004). See Appendix Supplementary Methods for details.

Electron microscopy

Autaptic neurons were fixed at DIV14–16 for 1–2 h at room temperature with 0.1 M cacodylate buffer/0.25 mM $CaCl_2$/0.5 mM $MgCl_2$ (pH 7.4) and processed as described (de Wit *et al*, 2006; Wierda *et al*, 2007). See Appendix Supplementary Methods for details.

Immunocytochemistry and confocal microscopy

Cultures were fixed at DIV14 with 4% formaldehyde and permeabilized with 0.5% Triton X-100. Neurons were stained with primary antibodies for 1 h at room temperature (RT), washed with phosphate-buffered saline, and stained for 1 h at RT with Alexa-conjugated secondary antibodies (1:1,000, Invitrogen). Coverslips were mounted with DABCO–Mowiol (Invitrogen) and examined on a Zeiss LSM510 confocal microscope. Images were acquired with a 40× oil objective (N.A. 1.3) and 0.7× mechanical zoom and analyzed in MATLAB with SynD (Schmitz *et al*, 2011). Somatic protein levels were quantified by placing six 10 × 10 pixel regions of interest (ROIs) in the cell soma. Synaptic protein levels were quantified by placing single ROIs on all VAMP2-positive synapses as described in Schmitz *et al* (2011).

Data representation and statistics

In all graphs, data are presented as mean values ± SEM. Statistical analysis was performed with SigmaPlot v11.0 (Systat software) or Instat v3.05 software (GraphPad software). *A priori* power calculations were performed using Excel (Microsoft). Data samples were tested for normal distribution with the Kolmogorov and Smirnov test and for heterogeneity of variance with the method of Bartlett. If allowed, an unpaired *t*-test (with Welch correction if required) was used. Alternatively, the nonparametric Mann–Whitney *U*-test was used to test for statistical significance. For multiple group comparisons, one-way ANOVA was used if allowed; otherwise, the nonparametric Kruskal–Wallis test was used. *P*-values below 0.05 are considered significant. In all experiments, the researcher was blinded to genotype or compound tested.

Expanded View for this article is available online.

Acknowledgements

We thank Hans Lodder, Roel van der Schors, and Jurjen Broeke for invaluable technical assistance; Robbert Zalm for cloning and viral production; Rien Dekker for electron microscopy; and Chris van der Meer, Joke Wortel, Joost Hoetjes, and Frank den Oudsten for breeding/genotyping mice. This work is supported by the EU (EU Synapse project 019055 to MV, EUROSPIN project HEALTH-F2-2009-241498 to MV, HEALTH-F2-2009-242167 SYNSYS project to MV, ABS, and KWL, Neuromics Marie Curie Early stage Training grant MEST-CT-2005-020919 to SKS) and by the Netherlands Organization for Scientific Research (ZonMw-VENI 916-66-101, ZonMW-TOP 91208017 to RFT; Pionier/VICI 900-01-001 and ZonMW 903-42-095 to MV). SKS is a recipient of a Netherlands Scientific Organization Toptalent grant (NWO 021.001.076).

Author contributions

SKS, MV and RFT designed research; IS, CKi and JTK performed biochemistry and immunocytochemistry; KWL and ABS performed mass spectrometry; HdW supervised electron microscopy; OS, SS, CKi and SKS performed behavioral

experiments; HDM supervised slice physiology experiments; LNC supervised autapse physiology experiments; SKS performed autapse electrophysiological recordings, autapse immunocytochemistry and biochemistry experiments; VH and DS performed electrophysiological recordings; CKo and TK performed slice electrophysiology recordings; JPH performed yeast two-hybrid screens; RFT, CKi and SKS analyzed the data; and SKS, MV and RFT wrote the manuscript.

Conflict of interest

The authors declare that they have no conflict of interest.

References

Abbott LF, Regehr WG (2004) Synaptic computation. *Nature* 431: 796 – 803

Alger BE (2002) Retrograde signaling in the regulation of synaptic transmission: focus on endocannabinoids. *Prog Neurobiol* 68: 247 – 286

Barbara JG, Auclair N, Roisin MP, Otani S, Valjent E, Caboche J, Soubrie P, Crepel F (2003) Direct and indirect interactions between cannabinoid CB1 receptor and group II metabotropic glutamate receptor signalling in layer V pyramidal neurons from the rat prefrontal cortex. *Eur J Neurosci* 17: 981 – 990

Boulton TG, Nye SH, Robbins DJ, Ip NY, Radziejewska E, Morgenbesser SD, DePinho RA, Panayotatos N, Cobb MH, Yancopoulos GD (1991) ERKs: a family of protein-serine/threonine kinases that are activated and tyrosine phosphorylated in response to insulin and NGF. *Cell* 65: 663 – 675

Burrone J, O'Byrne M, Murthy VN (2002) Multiple forms of synaptic plasticity triggered by selective suppression of activity in individual neurons. *Nature* 420: 414 – 418

Bushell TJ, Lee CC, Shigemoto R, Miller RJ (1999) Modulation of synaptic transmission and differential localisation of mGlus in cultured hippocampal autapses. *Neuropharmacology* 38: 1553 – 1567

Carr CM, Rizo J (2010) At the junction of SNARE and SM protein function. *Curr Opin Cell Biol* 22: 488 – 495

Castillo PE, Younts TJ, Chavez AE, Hashimotodani Y (2012) Endocannabinoid signaling and synaptic function. *Neuron* 76: 70 – 81

Chevaleyre V, Takahashi KA, Castillo PE (2006) Endocannabinoid-mediated synaptic plasticity in the CNS. *Annu Rev Neurosci* 29: 37 – 76

Chevaleyre V, Heifets BD, Kaeser PS, Sudhof TC, Castillo PE (2007) Endocannabinoid-mediated long-term plasticity requires cAMP/PKA signaling and RIM1alpha. *Neuron* 54: 801 – 812

Chi P, Greengard P, Ryan TA (2003) Synaptic vesicle mobilization is regulated by distinct synapsin I phosphorylation pathways at different frequencies. *Neuron* 38: 69 – 78

Cijsouw T, Weber JP, Broeke JH, Broek JA, Schut D, Kroon T, Saarloos I, Verhage M, Toonen RF (2014) Munc18-1 redistributes in nerve terminals in an activity- and PKC-dependent manner. *J Cell Biol* 204: 759 – 775

Dalton GD, Howlett AC (2012) Cannabinoid CB1 receptors transactivate multiple receptor tyrosine kinases and regulate serine/threonine kinases to activate ERK in neuronal cells. *Br J Pharmacol* 165: 2497 – 2511

Derkinderen P, Valjent E, Toutant M, Corvol JC, Enslen H, Ledent C, Trzaskos J, Caboche J, Girault JA (2003) Regulation of extracellular signal-regulated kinase by cannabinoids in hippocampus. *J Neurosci* 23: 2371 – 2382

Di Cristo G, Berardi N, Cancedda L, Pizzorusso T, Putignano E, Ratto GM, Maffei L (2001) Requirement of ERK activation for visual cortical plasticity. *Science* 292: 2337 – 2340

Ehlers MD (2003) Activity level controls postsynaptic composition and signaling via the ubiquitin-proteasome system. *Nat Neurosci* 6: 231 – 242

English JD, Sweatt JD (1996) Activation of p42 mitogen-activated protein kinase in hippocampal long term potentiation. *J Biol Chem* 271: 24329 – 24332

Fanselow MS, Dong HW (2010) Are the dorsal and ventral hippocampus functionally distinct structures? *Neuron* 65: 7 – 19

Ferraguti F, Baldani-Guerra B, Corsi M, Nakanishi S, Corti C (1999) Activation of the extracellular signal-regulated kinase 2 by metabotropic glutamate receptors. *Eur J Neurosci* 11: 2073 – 2082

Genc O, Kochubey O, Toonen RF, Verhage M, Schneggenburger R (2014) Munc18-1 is a dynamically regulated PKC target during short-term enhancement of transmitter release. *eLife* 3: e01715

Gomez N, Cohen P (1991) Dissection of the protein kinase cascade by which nerve growth factor activates MAP kinases. *Nature* 353: 170 – 173

Hartmann M, Heumann R, Lessmann V (2001) Synaptic secretion of BDNF after high-frequency stimulation of glutamatergic synapses. *EMBO J* 20: 5887 – 5897

Harvey CD, Yasuda R, Zhong H, Svoboda K (2008) The spread of Ras activity triggered by activation of a single dendritic spine. *Science* 321: 136 – 140

Heifets BD, Castillo PE (2009) Endocannabinoid signaling and long-term synaptic plasticity. *Annu Rev Physiol* 71: 283 – 306

Howe LR, Leevers SJ, Gómez N, Nakielny S, Cohen P, Marshall CJ (1992) Activation of the MAP kinase pathway by the protein kinase raf. *Cell* 71: 335 – 342

Jiang X, Litkowski PE, Taylor AA, Lin Y, Snider BJ, Moulder KL (2010) A role for the ubiquitin-proteasome system in activity-dependent presynaptic silencing. *J Neurosci* 30: 1798 – 1809

Jovanovic JN, Czernik AJ, Fienberg AA, Greengard P, Sihra TS (2000) Synapsins as mediators of BDNF-enhanced neurotransmitter release. *Nat Neurosci* 3: 323 – 329

Kamiya H, Shinozaki H, Yamamoto C (1996) Activation of metabotropic glutamate receptor type 2/3 suppresses transmission at rat hippocampal mossy fibre synapses. *J Physiol* 493(Pt 2): 447 – 455

Kellogg R, Mackie K, Straiker A (2009) Cannabinoid CB1 receptor-dependent long-term depression in autaptic excitatory neurons. *J Neurophysiol* 102: 1160 – 1171

Kreitzer AC, Regehr WG (2001) Retrograde inhibition of presynaptic calcium influx by endogenous cannabinoids at excitatory synapses onto Purkinje cells. *Neuron* 29: 717 – 727

Kreitzer AC, Regehr WG (2002) Retrograde signaling by endocannabinoids. *Curr Opin Neurobiol* 12: 324 – 330

Kushner SA, Elgersma Y, Murphy GG, Jaarsma D, Hojjati MR, Cui YJ, LeBoutillier JC, Marrone DF, Choi ES, De Zeeuw CI, Petit TL, Pozzo-Miller L, Silva AJ (2005) Modulation of presynaptic plasticity and learning by the H-ras/extracellular signal-regulated kinase/synapsin I signaling pathway. *J Neurosci* 25: 9721 – 9734

Kyriakis JM, App H, Zhang XF, Banerjee P, Brautigan DL, Rapp UR, Avruch J (1992) Raf-1 activates MAP kinase-kinase. *Nature* 358: 417 – 421

Lazarevic V, Schöne C, Heine M, Gundelfinger ED, Fejtova A (2011) Extensive remodeling of the presynaptic cytomatrix upon homeostatic adaptation to network activity silencing. *J Neurosci* 31: 10189 – 10200

Lee HG, Zhu X, Casadesus G, Pallas M, Camins A, O'Neill MJ, Nakanishi S, Perry G, Smith MA (2009) The effect of mGluR2 activation on signal transduction pathways and neuronal cell survival. *Brain Res* 1249: 244 – 250

Li KW, Miller S, Klychnikov O, Loos M, Stahl-Zeng J, Spijker S, Mayford M, Smit AB (2007) Quantitative proteomics and protein network analysis of hippocampal synapses of CaMKIIalpha mutant mice. *J Proteome Res* 6: 3127 – 3133

Macek TA, Winder DG, Gereau RW, Ladd CO, Conn PJ (1996) Differential involvement of group II and group III mGluRs as autoreceptors at

lateral and medial perforant path synapses. *J Neurophysiol* 76: 3798 – 3806

Marsicano G, Goodenough S, Monory K, Hermann H, Eder M, Cannich A, Azad SC, Cascio MG, Gutierrez SO, van der Stelt M, Lopez-Rodriguez ML, Casanova E, Schutz G, Zieglgansberger W, Di Marzo V, Behl C, Lutz B (2003) CB1 cannabinoid receptors and on-demand defense against excitotoxicity. *Science* 302: 84 – 88

Martin KC, Michael D, Rose JC, Barad M, Casadio A, Zhu H, Kandel ER (1997) MAP kinase translocates into the nucleus of the presynaptic cell and is required for long-term facilitation in Aplysia. *Neuron* 18: 899 – 912

Mateo Z, Porter JT (2007) Group II metabotropic glutamate receptors inhibit glutamate release at thalamocortical synapses in the developing somatosensory cortex. *Neuroscience* 146: 1062 – 1072

Misura KM, Scheller RH, Weis WI (2000) Three-dimensional structure of the neuronal-Sec1-syntaxin 1a complex. *Nature* 404: 355 – 362

Moulder KL, Jiang X, Taylor AA, Olney JW, Mennerick S (2006) Physiological activity depresses synaptic function through an effect on vesicle priming. *J Neurosci* 26: 6618 – 6626

Murthy VN, Schikorski T, Stevens CF, Zhu Y (2001) Inactivity produces increases in neurotransmitter release and synapse size. *Neuron* 32: 673 – 682

Ohno-Shosaku T, Tsubokawa H, Mizushima I, Yoneda N, Zimmer A, Kano M (2002) Presynaptic cannabinoid sensitivity is a major determinant of depolarization-induced retrograde suppression at hippocampal synapses. *J Neurosci* 22: 3864 – 3872

O'Leary DM, Cassidy EM, O'Connor JJ (1997) Group II and III metabotropic glutamate receptors modulate paired pulse depression in the rat dentate gyrus *in vitro*. *Eur J Pharmacol* 340: 35 – 44

Pinheiro PS, Mulle C (2008) Presynaptic glutamate receptors: physiological functions and mechanisms of action. *Nat Rev Neurosci* 9: 423 – 436

Pozo K, Goda Y (2010) Unraveling mechanisms of homeostatic synaptic plasticity. *Neuron* 66: 337 – 351

Rinetti GV, Schweizer FE (2010) Ubiquitination acutely regulates presynaptic neurotransmitter release in mammalian neurons. *J Neurosci* 30: 3157 – 3166

Rosenmund C, Stevens CF (1996) Definition of the readily releasable pool of vesicles at hippocampal synapses. *Neuron* 16: 1197 – 1207

Satoh Y, Endo S, Ikeda T, Yamada K, Ito M, Kuroki M, Hiramoto T, Imamura O, Kobayashi Y, Watanabe Y, Itohara S, Takishima K (2007) Extracellular signal-regulated kinase 2 (ERK2) knockdown mice show deficits in long-term memory; ERK2 has a specific function in learning and memory. *J Neurosci* 27: 10765 – 10776

Scanziani M, Salin PA, Vogt KE, Malenka RC, Nicoll RA (1997) Use-dependent increases in glutamate concentration activate presynaptic metabotropic glutamate receptors. *Nature* 385: 630 – 634

Schmitz SK, Hjorth JJ, Joemai RM, Wijntjes R, Eijgenraam S, de Bruijn P, Georgiou C, de Jong AP, van Ooyen A, Verhage M, Cornelisse LN, Toonen RF, Veldkamp WJ, Veldkamp W (2011) Automated analysis of neuronal morphology, synapse number and synaptic recruitment. *J Neurosci Methods* 195: 185 – 193

Segal RA, Greenberg ME (1996) Intracellular signaling pathways activated by neurotrophic factors. *Annu Rev Neurosci* 19: 463 – 489

Shuang R, Zhang L, Fletcher A, Groblewski GE, Pevsner J, Stuenkel EL (1998) Regulation of Munc-18/syntaxin 1A interaction by cyclin-dependent kinase 5 in nerve endings. *J Biol Chem* 273: 4957 – 4966

Stiedl O, Tovote P, Ögren SO, Meyer M (2004) Behavioral and autonomic dynamics during contextual fear conditioning in mice. *Auton Neurosci Basic Clin* 115: 15 – 27

Straiker A, Mackie K (2005) Depolarization-induced suppression of excitation in murine autaptic hippocampal neurones. *J Physiol* 569: 501 – 517

Südhof TC, Rothman JE (2009) Membrane fusion: grappling with SNARE and SM proteins. *Science* 323: 474 – 477

Sullivan JM (2007) A simple depletion model of the readily releasable pool of synaptic vesicles cannot account for paired-pulse depression. *J Neurophysiol* 97: 948 – 950

Thomas GM, Huganir RL (2004) MAPK cascade signalling and synaptic plasticity. *Nat Rev Neurosci* 5: 173 – 183

Toonen RF, de Vries KJ, Zalm R, Südhof TC, Verhage M (2005) Munc18-1 stabilizes syntaxin 1, but is not essential for syntaxin 1 targeting and SNARE complex formation. *J Neurochem* 93: 1393 – 1400

Toonen RFG, Wierda K, Sons MS, de Wit H, Cornelisse LN, Brussaard A, Plomp JJ, Verhage M (2006) Munc18-1 expression levels control synapse recovery by regulating readily releasable pool size. *Proc Natl Acad Sci USA* 103: 18332 – 18337

Toonen RF, Verhage M (2007) Munc18-1 in secretion: lonely Munc joins SNARE team and takes control. *Trends Neurosci* 30: 564 – 572

Turrigiano GG, Leslie KR, Desai NS, Rutherford LC, Nelson SB (1998) Activity-dependent scaling of quantal amplitude in neocortical neurons. *Nature* 391: 892 – 896

Turrigiano G (2011) Too many cooks? Intrinsic and synaptic homeostatic mechanisms in cortical circuit refinement. *Annu Rev Neurosci* 34: 89 – 103

Vara H, Onofri F, Benfenati F, Sassoè-Pognetto M, Giustetto M (2009) ERK activation in axonal varicosities modulates presynaptic plasticity in the CA3 region of the hippocampus through synapsin I. *Proc Natl Acad Sci USA* 106: 9872 – 9877

Verhage M, Maia AS, Plomp JJ, Brussaard AB, Heeroma JH, Vermeer H, Toonen RF, Hammer RE, van den Berg TK, Missler M, Geuze HJ, Südhof TC (2000) Synaptic assembly of the brain in the absence of neurotransmitter secretion. *Science* 287: 864 – 869

Weber JP, Reim K, Sorensen JB (2010) Opposing functions of two sub-domains of the SNARE-complex in neurotransmission. *EMBO J* 29: 2477 – 2490

Wierda KDB, Toonen RFG, de Wit H, Brussaard AB, Verhage M (2007) Interdependence of PKC-dependent and PKC-independent pathways for presynaptic plasticity. *Neuron* 54: 275 – 290

Willeumier K, Pulst SM, Schweizer FE (2006) Proteasome inhibition triggers activity-dependent increase in the size of the recycling vesicle pool in cultured hippocampal neurons. *J Neurosci* 26: 11333 – 11341

Wilson RI, Kunos G, Nicoll RA (2001) Presynaptic specificity of endocannabinoid signaling in the hippocampus. *Neuron* 31: 453 – 462

Wilson RI, Nicoll RA (2001) Endogenous cannabinoids mediate retrograde signalling at hippocampal synapses. *Nature* 410: 588 – 592

Wilson RI, Nicoll RA (2002) Endocannabinoid signaling in the brain. *Science* 296: 678 – 682

Wiltgen BJ, Sanders MJ, Behne NS, Fanselow MS (2001) Sex differences, context preexposure, and the immediate shock deficit in Pavlovian context conditioning with mice. *Behav Neurosci* 115: 26 – 32

de Wit H, Cornelisse LN, Toonen RF, Verhage M (2006) Docking of secretory vesicles is syntaxin dependent. *PLoS ONE* 1: e126

Xu JY, Chen R, Zhang J, Chen C (2010) Endocannabinoids differentially modulate synaptic plasticity in rat hippocampal CA1 pyramidal neurons. *PLoS ONE* 5: e10306

Zhu JJ, Qin Y, Zhao M, Van Aelst L, Malinow R (2002) Ras and Rap control AMPA receptor trafficking during synaptic plasticity. *Cell* 110: 443 – 455

